Supporting Information

Wang et al. 10.1073/pnas.1616540113

Measurements of SO_2, NO_x (NO and NO_2), O_3, and $PM_{2.5}$
Ambient concentrations of SO_2, NO_x (NO and NO_2), and O_3 at the two sites in Xi'an and Beijing were measured with a time resolution of 15 min by using the Chemiluminescence nitrogen oxides analyzer (Ecotech EC9841), sulfur dioxide analyzer (Ecotech EC9852), and ozone monitor (Ecotech EC9810), respectively (21, 54). The in situ mass concentration of $PM_{2.5}$ in Xi'an was measured using the USA EPA-method E-BAM (Met One Instruments, Inc., USA) system (BX-802, Met One, Inc., Grants Pass, OR, USA), while in situ mass concentrations of $PM_{2.5}$ in Beijing was measured by using a heated Tapered Element Oscillating Microbalance system (TEOM series1400a, Thermo Scientific) (21). Both systems were operated under a flow rate of 16.7 L min^{-1} with a $PM_{2.5}$ inlet. Meteorological parameters such as temperature, visibility, and relative humidity were simultaneously measured.

Measurements of gaseous NH_3 and HONO and aerosol-phase ($PM_{2.5}$) inorganic ions in Xi'an
Concentrations of gaseous NH_3 and HONO and inorganic ions (i.e., SO_4^{2-}, NO_3^-, Cl^-, NH_4^+, Na^+, K^+, Mg^{2+}, and Ca^{2+}) in $PM_{2.5}$ were measured on-line with a time resolution of 1 hr by using Monitor for Aerosols and Gases in ambient air (MARGA, Metrohm Co., Switzerland), which is widely used for in situ measurements of both gaseous and particle-phase acidic and basic species (55, 56).

$PM_{2.5}$ filter sample collection and analysis
$PM_{2.5}$ filter sample collection was simultaneously performed in Xi'an from 5 to 12 December 2012 using two high-volume samplers and one mini-volume sampler. The high-volume $PM_{2.5}$ samples were collected onto pre-combusted (450°C, 8 hrs) quartz fiber filter (Whatman 400, USA) at a flow rate of 1.13 m^3 min^{-1} and a time resolution of 1 hr, while the mini-volume $PM_{2.5}$ samples were collected onto PTFE filters (Φ47mm) at a flow rate of 5 L min^{-1} on a day/night basis. After sampling, all filter samples were sealed in an aluminum foil bag individually and stored in a freezer under −20°C prior to analysis. The high-volume $PM_{2.5}$ filter samples were analyzed for elemental carbon (EC) and organic carbon (OC) by a Desert Research Institute (DRI) carbon analyzer (57), while the mini-volume $PM_{2.5}$ samples were determined for the total Fe and Mn and their water-soluble fractions (58, 59).

NH_3 and PM_1 chemical composition in Beijing
Concentrations of gaseous NH_3 in Beijing were measured using the same method as that in Xi'an 2012. The chemical composition of PM_1 in Beijing 2015 was measured by an Aerodyne high-resolution time-of-flight aerosol mass spectrometer (21). Since sulfate exists dominantly in fine aerosols, the difference in the SO_4^{2-} content between PM_1 and $PM_{2.5}$ is small, i.e., typically less than 15% in Beijing (21).

Particle acidity (pH) calculation
The pH value of particles was determined by utilizing the ISORROPIA-II model, a subroutine commonly used in large-scale chemical transport models that incorporates both gaseous and particle-phase measurements. An accurate estimate of particle acidity is determined to a high degree of accuracy on the basis of measurements of semivolatile partitioning of certain species (e.g., NH_3/NH_4^+) (28, 60). ISORROPIA-II calculates the equilibrium concentration of an aerosol composed of inorganic species (NH_4^+, Na^+, K^+, Mg^{2+}, Ca^{2+}, SO_4^{2-}, NO_3^-, and Cl^-) and water. In this study, the ISORROPIA-II model was run in the forward mode (i.e., incorporating the gas and aerosol measurements). The pH calculation utilized measurements of NH_3, NH_4^+, Na^+, K^+, Mg^{2+}, Ca^{2+}, SO_4^{2-}, NO_3^-, and Cl^- for Xi'an 2012 and NH_3, NH_4^+, SO_4^{2-}, NO_3^-, and Cl^- for Beijing 2015. For both field campaigns, the predicted NH_3 concentration by the ISORROPIA-II model was closely correlated with the field measurements (i.e., $R^2 = 0.95$ with $y=1.07x + 0.69$ and $y = 1.07x + 1.07$ for Xi'an 2012 and Beijing 2015, respectively) (Fig. S12).

Aqueous SO_2 oxidation by NO_2 on bulk solutions in a reaction cell
Laboratory experiments were performed to evaluate SO_2 oxidation by NO_2 on bulk solutions in a 125 mL reaction cell. SO_2 and NO_2 in N_2 or pure air was introduced into the reaction cell and exposed to a 2 mL of pure water or 3 wt % NH_3 solution, which was placed at the bottom of the reaction cell. The entire reaction cell was covered by aluminum foil and maintained at the room temperature (~298 K). After exposure over a period of 8 hrs, 1 μL of the exposed solution from the reaction cell was analyzed by a thermal desorption-ion drift-chemical ionization mass spectrometer (TD-ID-CIMS) for sulfate formation.

The integrated desorption peak area of the sulfate signal (detected as SO_4^{2-} at m/z=96 by TD-ID-CIMS, Fig. S9A) confirms that dissolved SO_2 in pure water is oxidized into SO_4^{2-} by dissolved NO_2. For the exposure of SO_2 and NO_2 to 3 wt % NH_3 solution, the integrated peak area of sulfate signal is increased by about a factor of two (Table S3), suggesting that the oxidation is enhanced under a high pH condition. Also, there is little difference in the measured integrated peak areas of sulfate signal for exposures using N_2 and air as the buffer gas under similar conditions, suggesting that the role of O_2 in the conversion of SO_2 into SO_4^{2-} is insignificant. Furthermore, there is no detectable sulfate signal (i.e., close to the background level) with only SO_2 exposure (in the absence of NO_2) to pure water or 3 wt % NH_3 solution under similar conditions.

Aqueous SO_2 oxidation by NO_2 on particles in a reaction chamber

We conducted experiments by exposing seed particles to SO_2, NO_2, and NH_3 at variable RH and measuring the dry size variation and sulfate formation on the exposed particles in a 1 m^3 Teflon reaction chamber covered with aluminum foil (Fig. S10). Prior to each experiment, the chamber was flushed by pure N_2 three times to remove residual particles and other contaminants. Water vapor in the reaction chamber was provided from a 5-gallon water reservoir equipped with a water heater set at 307 K. A 2 SLPM nitrogen flow passed through the water reservoir to produce a humidified nitrogen flow that was subsequently introduced into the chamber. The RH in the chamber was monitored using a 24 V (DC) RH probe located downstream of the chamber. A differential mobility analyzer (DMA) equipped with a condensation particle counter (CPC) and a TD-ID-CIMS was employed to measure the size distribution and chemical compositions of aerosols, respectively, before and after the exposure. Size-selected (45 nm) oxalic acid particles were used as model particles in the reaction chamber for the aqueous conversion of SO_2 to sulfate. Oxalic acid particles were generated by utilizing a continuous flow particle generator (TSI 3076) to atomize an aqueous solution of oxalic acid (1 wt %). The particle flow was diluted with dry nitrogen at a 4:1 ratio. Poly-dispersed seed particles were heated to 343 K to remove excess humidity from the flow and further dried using two Nafion tubes (PD-070−18T-12SS, Perma Pure). Particles were then charged by a ^{210}Po radioactive source and size selected by the DMA. A condensation particle counter (CPC, TSI 3762) was utilized for particle concentration measurement. Typically, the size selected particle number concentration inside the chamber was elevated to 5×10^4 cm^{-3} before gases were injected. SO_2 was from Sigma-Aldrich, and NO_2 and NH_3 were from Matheson. Gas samples of SO_2 and NO_2 were injected into the chamber from pressurized lecture bottles utilizing a mass flow controller to monitor the flow of gas into the chamber. The concentrations in the lecture bottles were prepared by diluting SO_2 or NO_2 with dry nitrogen. SO_2, NO_2, and NH_3 were introduced separately into the reaction chamber with the initial concentrations of 250 ppb, 250 ppb, and 1ppm, and their concentrations were monitored by a SO_2 analyzer, a NO_x analyzer, and ID-CIMS (61-63), respectively. The particles and gas mixture were allowed to react for about 1 hr before measuring the size distribution and chemical compositions of particles. The exposed particles were then introduced into the DMA to determine the variation in the dry particle size; particles were heated to 343 K to remove excess humidity from the flow, further dried using the two Nafion tubes, and charged by a ^{210}Po radioactive source. The particle size distribution was determined by the DMA. To analyze the chemical composition, the exposed particles were introduced to an electrostatic particle collector (EPC) of the TD-ID-CIMS and then to the CPC. The TD-ID-CIMS equipped with the EPC was capable of collecting aerosols from 2 to 200 nm. The aerosol flow crossed the EPC at 1.5 SLPM with a dry nitrogen sheath flow of 0.3 SLPM. The particle flow passed through the EPC, and particles were collected using a voltage of 3300 V (DC) on a platinum based collection/desorption filament. After collection, the particle sample was introduced into the ionization chamber, and the filament was heated to 600 K to evaporate the sample by applying a 2 V (AC) voltage. Chemical ionization was achieved by utilizing the CO_3^- /CO_4^- ionization scheme to generate negative ions for the negative mode mass spectrometry. Mass spectrometry analysis was made using a triple quadrupole (QqQ) Extrel ELQ 400 instrument by utilizing Selected Ion Monitoring (SIM) for the ions of interest (i.e., sulfate or oxalic acid). Fig. S9A illustrates the mass spectrometry analysis for an ammonium sulfate standard solution, showing three major peaks for the sulfate ion SO_4^{2-} at m/z = 96, the bisulfate ion HSO_4^- at m/z = 97, and the oxygen adduct of $SO_3 \bullet O_2^-$ at m/z = 122. The sulfate ion peak at m/z = 96 was employed in our analysis for the integrated peak area of the collected particles. Fig. S9B depicts the TD-ID-CIMS analysis of oxalic acid particles after exposure to the gas mixture of SO_2, NO_2, and NH_3 at 65 % RH, with a change in diameter from 45 to 75 nm. The mass spectrometry analysis shows that collected particles contain both oxalic acid and sulfate, i.e., with the ions at m/z = 89, 96, 97, 112, and 122 for [oxalic acid-H]$^-$, SO_4^{2-}, HSO_4^-, $SO_3 \bullet O_2^-$, and oxalic acid$\bullet O_2^-$, respectively.

Our results demonstrate a distinction for the experiments between bulk solutions and aerosols, showing that the aqueous SO_2 oxidation by NO_2 occurs with and without NH_3 on bulk solutions, but only in the presence of NH_3 on sub-micron particles. Our measured SO_4^{2-} formation after exposure to SO_2 and NO_2 on pure water solution (Table S3) is in agreement with the previous experimental studies showing sulfate production from the reaction of NO_2 with dissolved SO_3^{2-} or HSO_3^- ions in aqueous solutions (17-19). The higher sulfate formation by dissolution of ammonia (at a higher pH) is consistent with a previous study of enhanced sulfate formation with NaCl and $NaNO_3$ salts exposed to a SO_2/NH_3/air mixture (35). In contrast, no observable particle growth nor sulfate formation is measured on seed oxalic acid particles exposed to SO_2 and NO_2 in the absence of NH_3 (Table S4), because of highly elevated particle acidity. Also, there is no observable particle growth or sulfate formation when oxalic acid particles are exposed to SO_2 and NH_3 but in the absence of NO_2 at 70% RH (Table S4). This implies that growth of oxalic acid particles by NH_3 neutralization alone is negligible, consistent with a previous study of little size growth of sulfuric acid nanoparticles after NH_3 exposure at high concentrations (30).

Estimation of SO_2 uptake coefficient

The production rate of sulfate by the aqueous oxidation of SO_2 by NO_2 on particles is approximated by (64),

$$\frac{d[SO_4^{2-}]}{dt} \approx \frac{1}{4}\Upsilon\bar{C}S[SO_2(g)] \qquad (1)$$

where $d[SO_4^{2-}]$ is the molar concentration of sulfate produced during the time period of dt, γ is the effective uptake coefficient, $\bar{C}$is the mean molecular speed, S is the aerosol surface to volume ration, and $[SO_2(g)]$ is the gaseous SO_2 concentration. The γ values were determined from equation (1), using the gaseous and particle properties measured from the field campaign and reaction chamber study (Tables S5 and S6). For the Beijing 2015, we identified the pollution events and divided each event

into the clean, transition, and polluted periods (as in Fig. 1) on the basis of the sulfate mass concentration. The γ value was calculated for the each period of an individual event using the mean values of the particle size (D_p), number concentration (N), sulfate mass growth ($d[SO_4^{2-}]$), gas-phase SO_2 concentration ($[SO_2(g)]$), and the particle growth time (dt). In the reaction chamber experiments, the measured particle growth factor (Fig. 3C) was employed to derive the γ values at different RH levels.

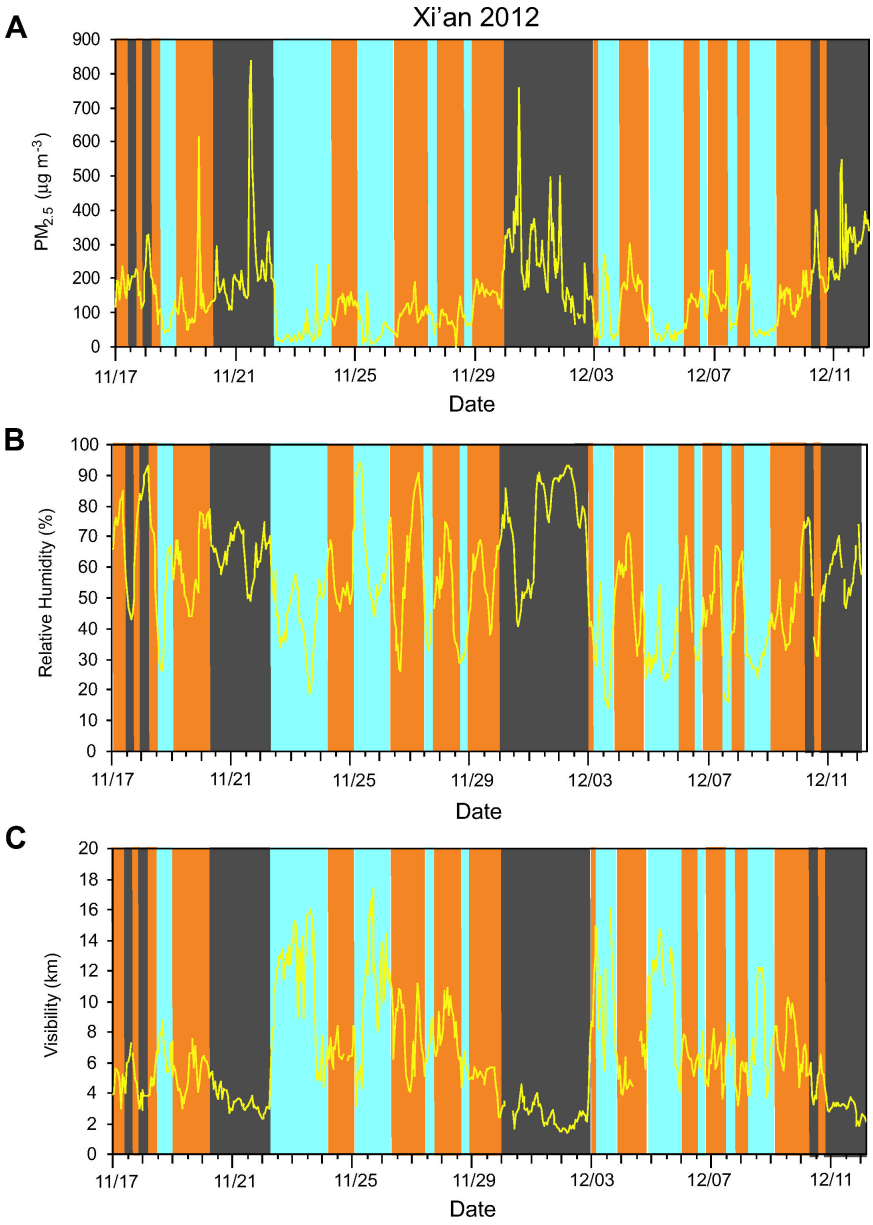

Fig. S1. $PM_{2.5}$ and meteorological conditions in Xi'an. (*A* to *C*) Temporal evolutions of $PM_{2.5}$ mass concentration, relative humidity, and visibility, respectively. The shaded colors are defined similarly to those in Fig. 1.

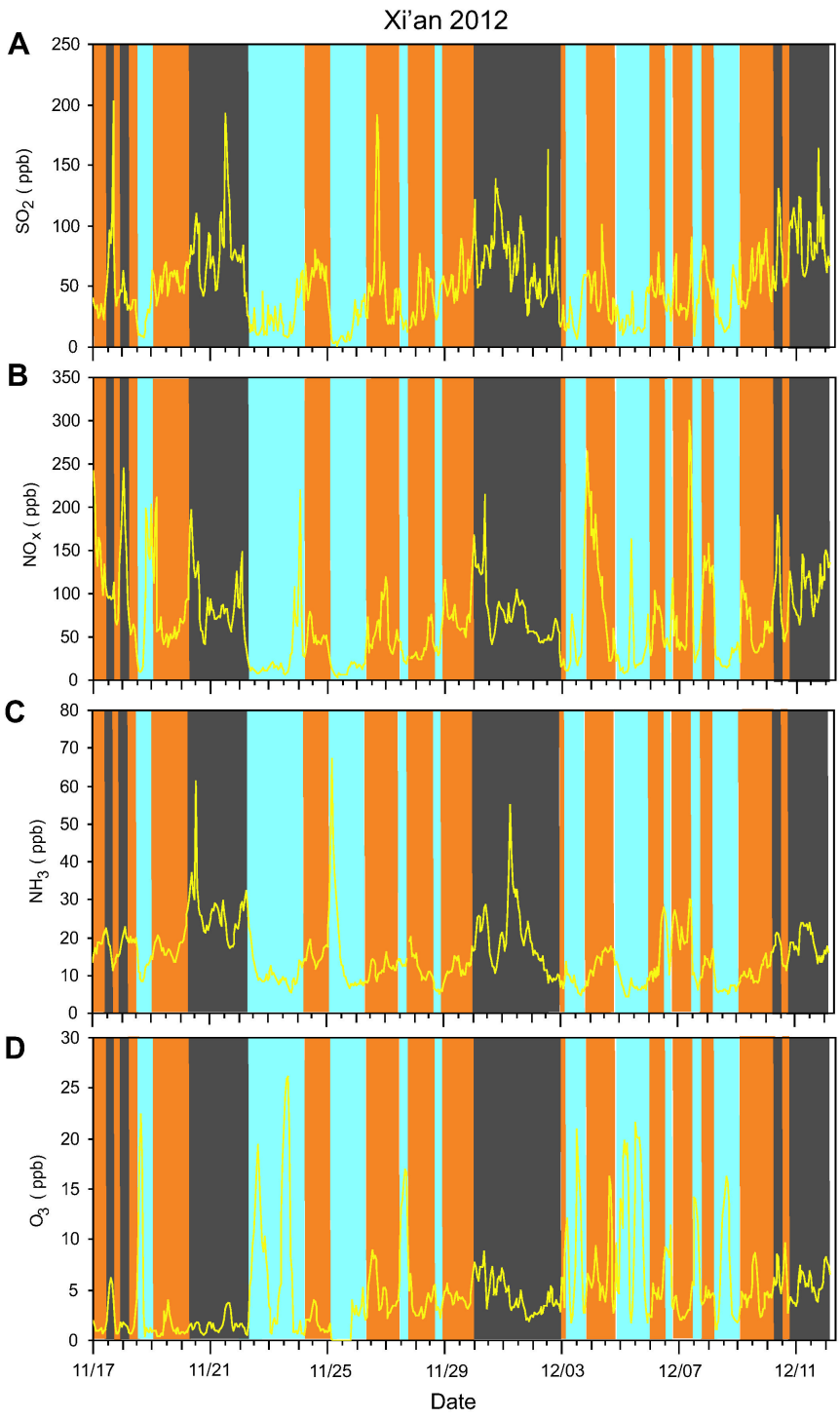

Fig. S2. Gaseous pollutants in Xi'an. (*A* to *D*) Temporal evolutions of SO_2, NO_x, NH_3, and O_3, respectively. The shaded colors are defined similarly to those in Fig. 1.

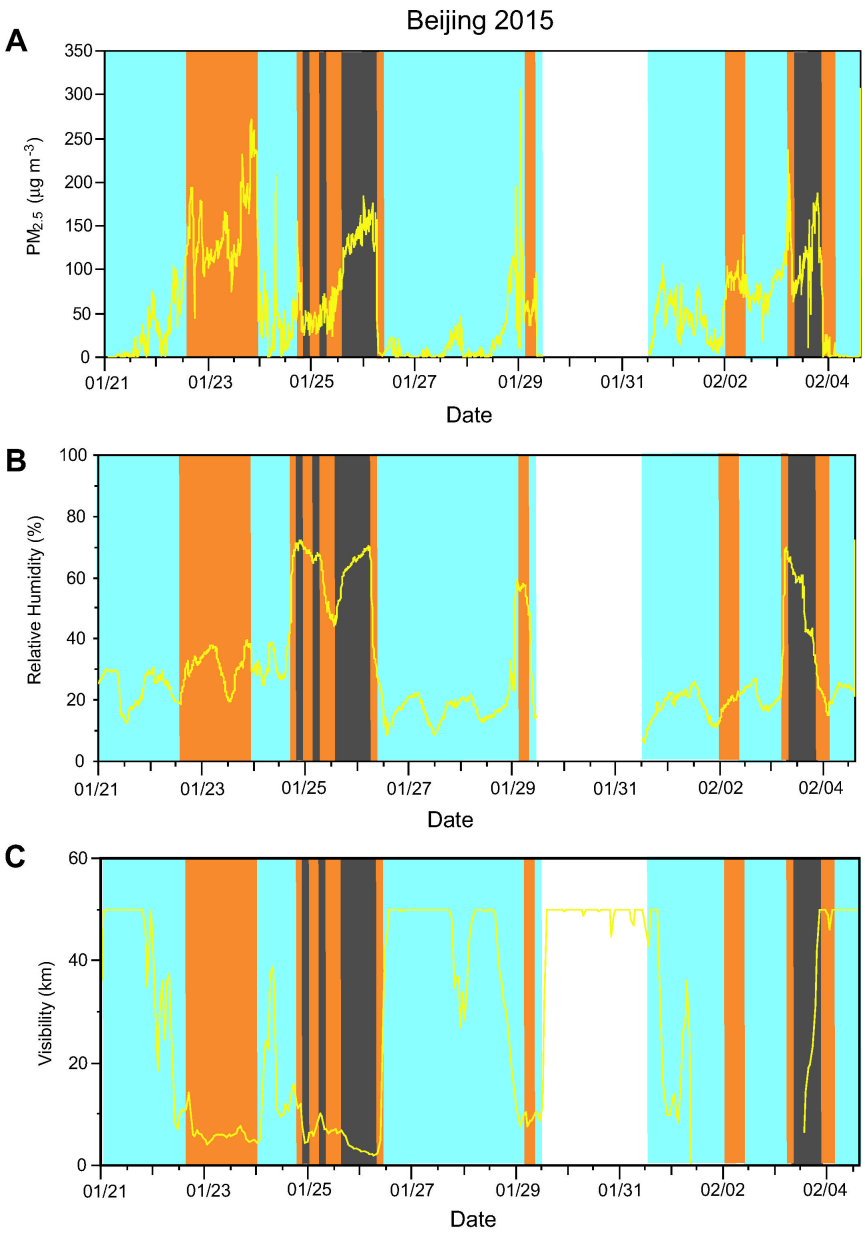

Fig. S3. $PM_{2.5}$ and meteorological conditions in Beijing. (*A* to *C*) Temporal evolutions of $PM_{2.5}$ mass concentration, relative humidity, and visibility, respectively. The shaded colors are defined similarly to those in Fig. 1.

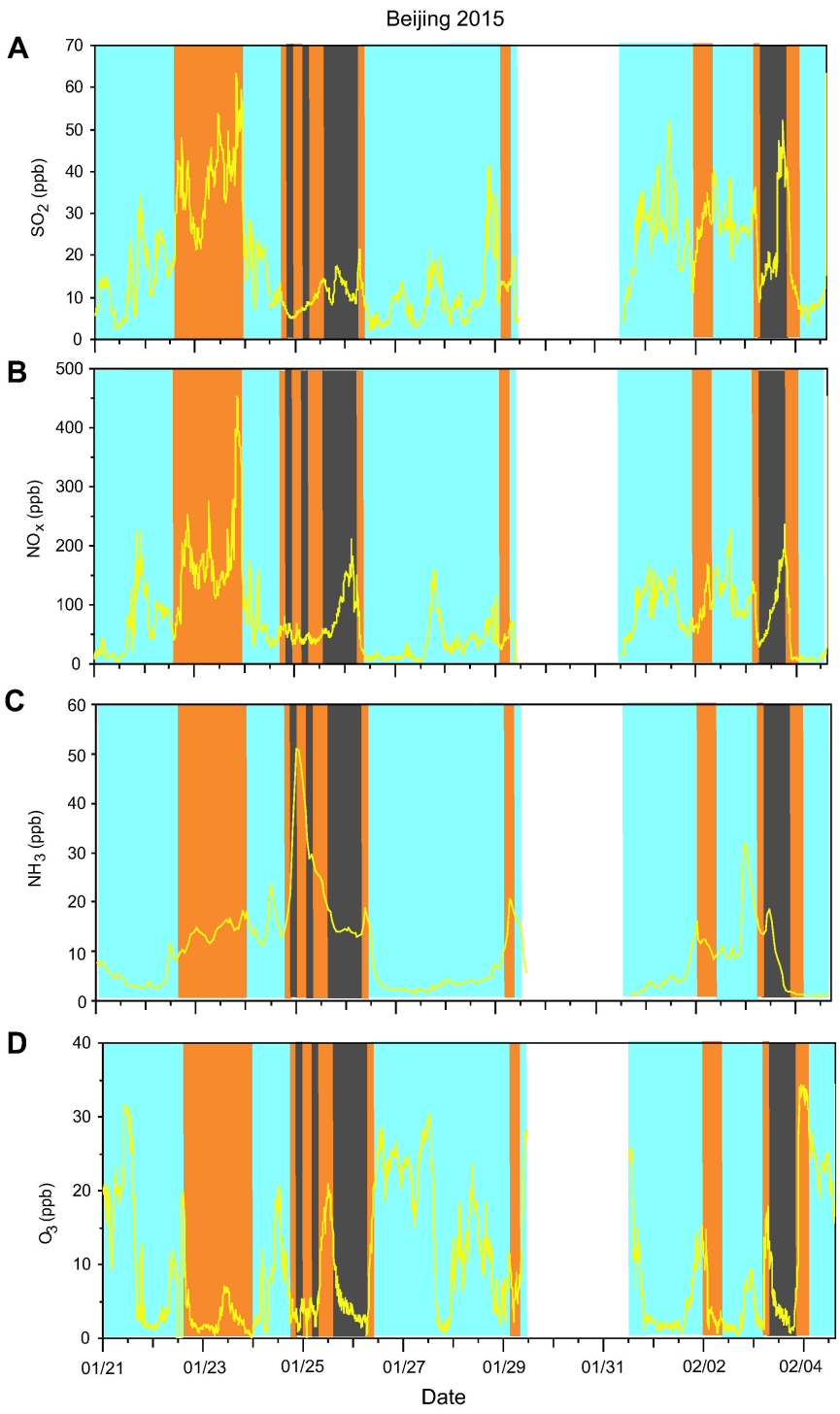

Fig. S4. Gaseous pollutants in Beijing. (*A* to *D*), Temporal evolutions of SO_2, NO_x, NH_3, and O_3, respectively. The shaded colors are defined similarly to those in Fig. 1.

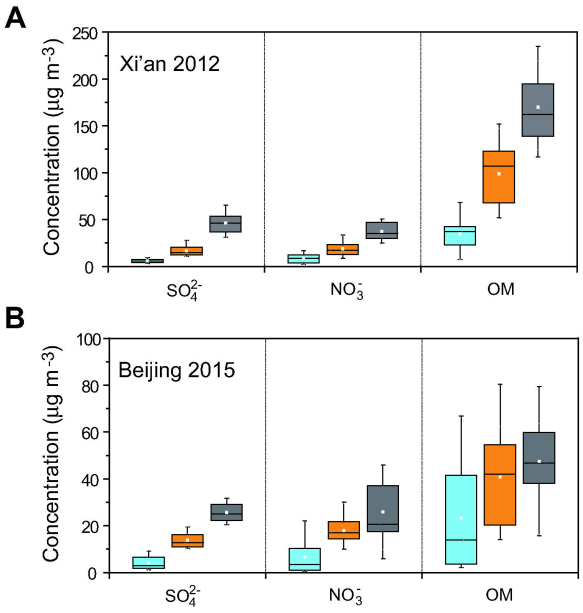

Fig. S5. PM growth in Xi'an and Beijing. Mass concentrations of SO_4^{2-}, NO_3^-, and OM in Xi'an (*A*) and Beijing (*B*).

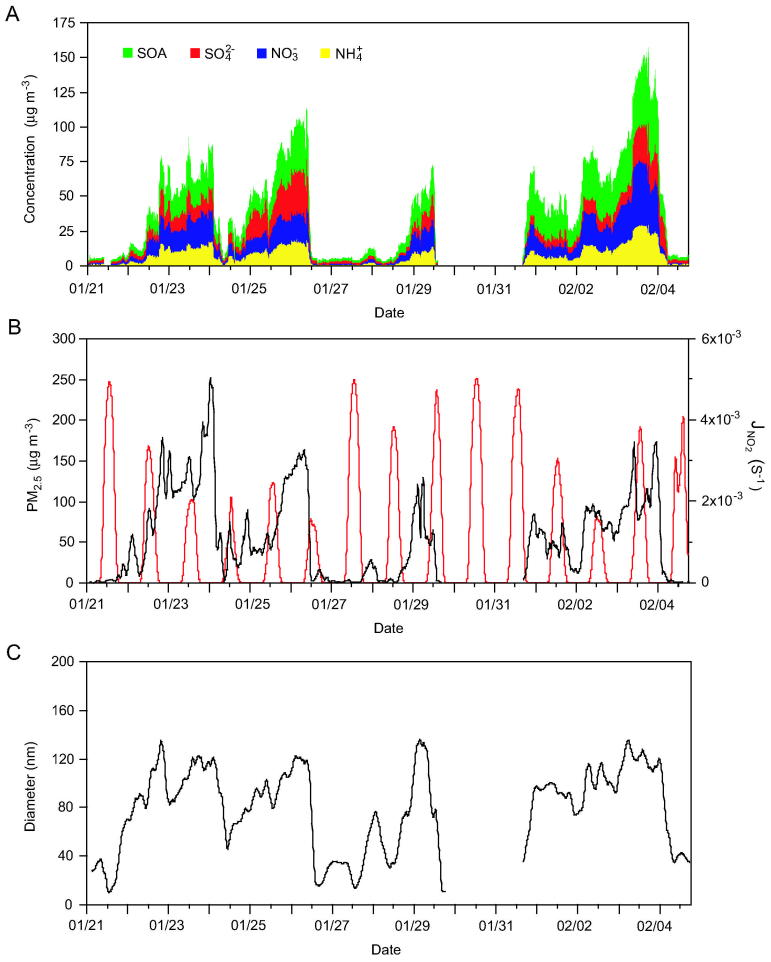

Fig. S6. Photochemistry vs PM production in Beijing. Temporal evolutions of SOA, SO_4^{2-}, NO_3^-, and NH_4^+ mass concentrations (*A*), $PM_{2.5}$ (black, left axis) and J_{NO2} (red, left axis) (*B*), and the average particle diameter (*C*).

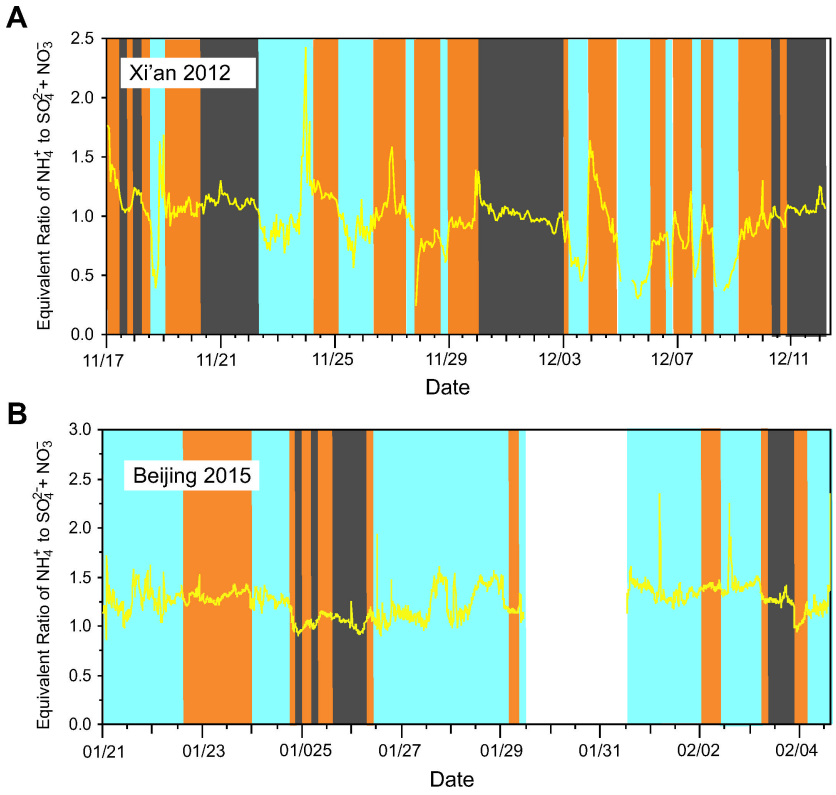

Fig. S7. Ratio of NH_4^+ to SO_4^{2-} and NO_3^-. (*A* and *B*) Temporal evolutions of the equivalent ratio of NH_4^+ to the sum of SO_4^{2-} and NO_3^- during Xi'an and Beijing, respectively. The shaded colors are defined similarly to those in Fig. 1.

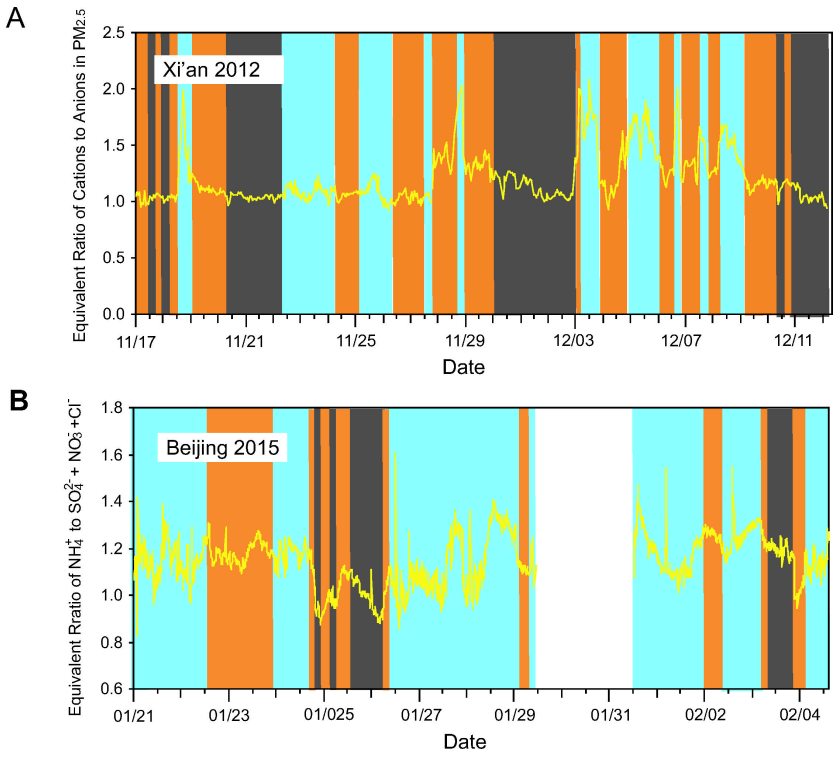

Fig. S8. Ratios of total non-proton cations to anions and NH_4^+ to SO_4^{2-}, NO_3^-, and Cl. (*A* and *B*) Temporal evolutions of the equivalent ratios of cations to anions in $PM_{2.5}$ in Xi'an and ammonium to the sum of sulfate, nitrate, and chloride in PM_1 in Beijing, respectively. The shaded colors are defined similarly to those in Fig. 1.

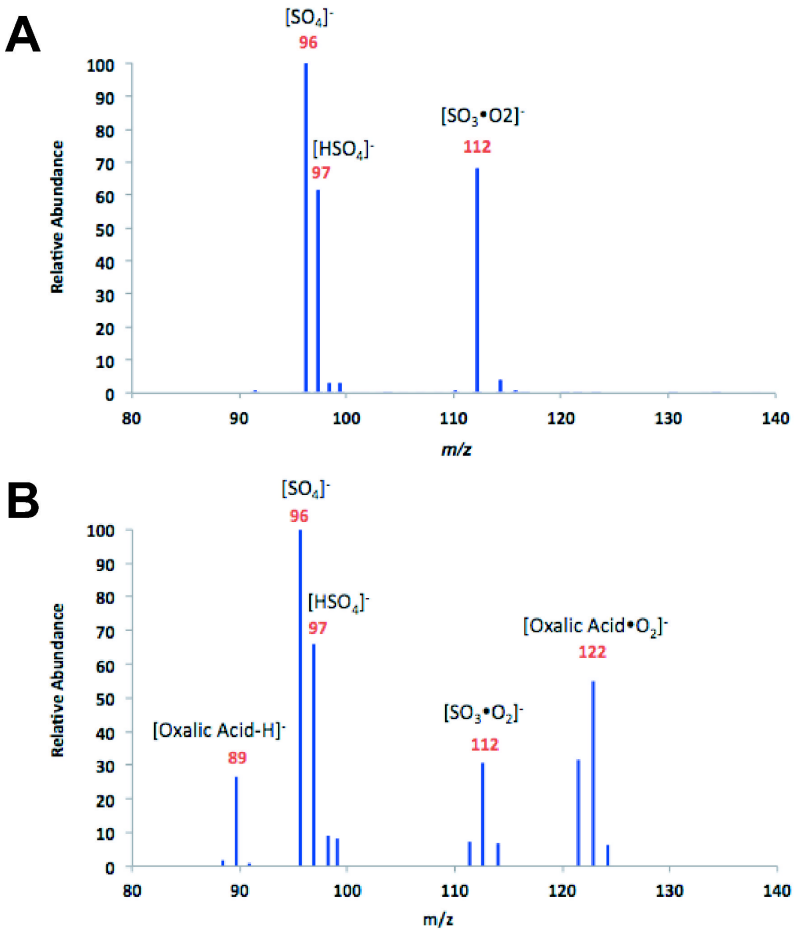

Fig. S9. Mass spectrometric sulfate detection. (A) Representative TD-ID-CIMS spectra of a $(NH_4)_2SO_4$ solution. (B) TD-ID-CIMS spectra of collected oxalic acid particles after exposure to SO_2, NO_2, and NH_3 at 65 % RH.

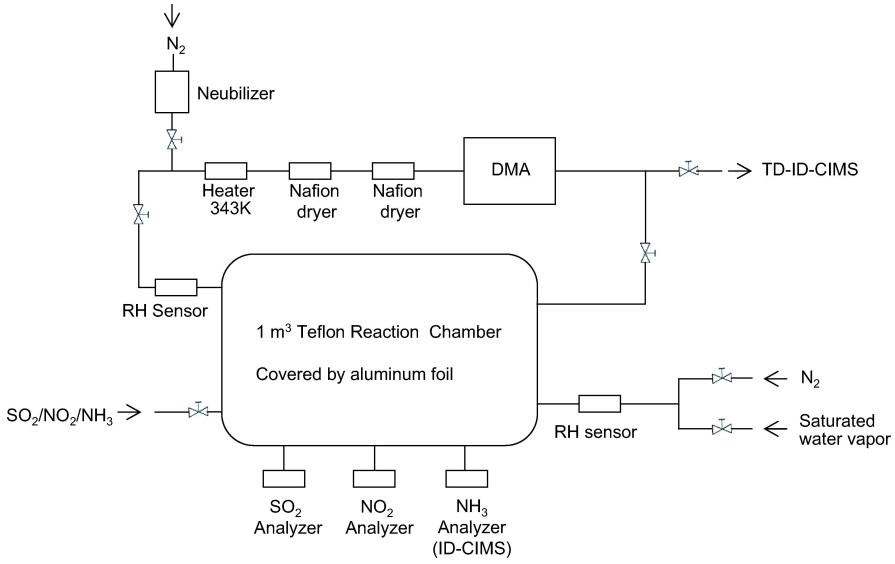

Fig. S10. Schematic representation of the reaction chamber. A 1 m^3 Teflon reaction chamber equipped with DMA and TD-ID-CIMS for detection of the variations in particle size and chemical compositions, respectively.

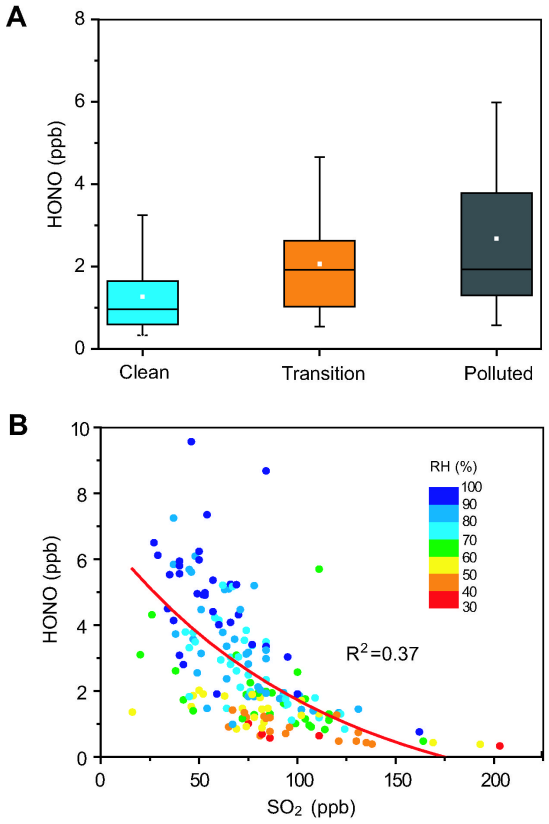

Fig. S11. Measurements of gaseous HONO in Xi'an. (*A*) Concentrations of gaseous HONO during the clean, transition and polluted periods. The shaded colors are defined similarly to those in Fig. 1. (*B*) Correlation between HONO, RH, and SO_2.

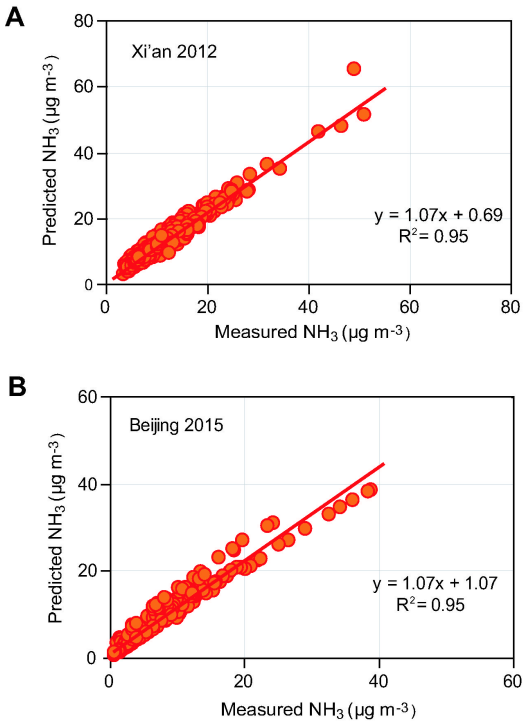

Fig. S12. Comparison between measured and predicted NH_3. (A and B) Concentrations of NH_3 measured and calculated using ISORROPIA-II in Xi'an 2012 (A) and Beijing 2015 (B).

Table S1. Gaseous and PM pollutants and meteorological parameters during Xi'an 2012

	Clean		Transition		Polluted	
	Mean	Range	Mean	Range	Mean	Range
I. Gaseous pollutants (ppb)						
SO_2	28±17	1.0−86	54±22	17−191	78±31	16−203
NO_X	44±49	5.0−264	76±51	15−300	92±39	25−245
O_3	7.4±7.0	0.0−26	4.1±4.7	0.4−11	4.1±2.4	0.6−9.6
NH_3	12±7.4	4.7−67	17±7.7	7.6−35	23±8.3	9.3−61
HONO	1.3±1.0	0.2−5.4	2.1±1.3	0.2−6.5	2.7±1.8	0.3−10
II. Inorganic ions, Fe, Mn and organic matter in $PM_{2.5}$ (μg m^{-3})						
SO_4^{2-}	5.9±2.2	2.3−10	14±4.4	10−20	38±14	20−83
NO_3^-	8.7±4.9	1.4−25	16±6.7	3.8−35	33±10	12−55
Cl^-	4.0±3.7	0.0−22	9.8±5.1	2.4−28	14±6.3	2.6−34
NH_4^+	4.0±2.2	0.8−11	10±3.7	5.1−18	25±7.7	3.2−44
Na^+	3.6±3.2	0.2−8.4	4.5±3.2	0.5−17	4.2±2.7	0.5−17
K^+	1.3±0.7	0.3−4.1	3.1±1.2	1.3−7.0	4.6±1.4	1.8−8.3
Mg^{2+}	0.2±0.1	0.1−0.7	0.3±0.1	0.0−0.7	0.3±0.1	0.0−0.8
Ca^{2+}	1.6±1.0	0.3−6.3	2.4±1.2	0.0−5.3	2.3±1.2	0.2−5.9
Total ions	29±13	6.8−63	60±19	34−97	121±32	65−199
Fe (μg m^{-3})	0.82±0.29	0.37−1.13	1.51±0.70	0.60−3.0	1.76±0.66	0.79−2.79
Mn (μg m^{-3})	0.04±0.04	0.00−0.10	0.11±0.08	0.04−0.35	0.15±0.07	0.08−0.29
Water-soluble Fe (ng m^{-3})	1.5±2.1	0.0−6.1	4.6±3.9	0.0−14	16±5.1	7.3−23
Water-soluble Mn (ng m^{-3})	10±2.1	3.8−20	21±8.7	11−40	41±16	17−70
Organic matter (OM)	35±15	7.0−70	99±33	38−163	177±39	116−288
pH	6.70±1.40	4.43-11.0	6.04±1.24	4.16-8.03	6.96±1.33	4.14-8.16
III. $PM_{2.5}$ and meteorological parameters						
$PM_{2.5}$ (μg m^{-3})	43±18	8.0−74	139±65	76−613	250±120	101−839
T (^OC)	5.7±4.1	-2.0−17	4.1±4.0	-2.3−11	4.1±4.4	-3.1−14
RH (%)	46±18	14−94	56±17	26−93	68±14	41−93
Visibility (km)	8.9±3.4	3.2−17	6.1±2.8	2.4−12	3.2±1.1	1.4−7.2

Table S2. Summary of gaseous and PM pollutants and meteorological parameters during Beijing 2015

	Clean		Transition		Polluted	
	Mean	Range	Mean	Range	Mean	Range
I. Gaseous pollutants (ppb)						
SO_2	16±10	16.9−52	26±15	5.1−63	18±11	5.16−52
NO_X	64±51	4.5−224	116±90	7.2−453	91±51	7.7−236
O_3	11±9.3	0.2−33	5.9±6.6	0.3−34	6.8±7.8	0.3−34
NH_3	6.4±5.1	0.9−27	18±11	4.4−51	17±5.7	10−32
II. Major inorganic ions and organic matter in PM_1 (μg m^{-3})						
Organic matter (OM)	23±23	1.0−102	41±21	8.0−94	47±18	14−90
SOA	9.6±9.3	0.5−35	19±6.9	7.9−45	31±10	12−53
SO_4^{2-}	4.2±2.7	0.3−10	14±3.1	10−20	26±3.9	20−38
NO_3^-	6.6±7.0	0.1−30	18±6.4	1.9−44	26±13	4.5−48
Cl^-	0.8±0.9	0.0−7.0	1.6±1.0	0.0−5.1	1.7±0.9	0.0−4.5
NH_4^+	4.7±3.1	0.2−18	13±3.5	5.1−26	20±6.2	9.1−30
pH	-	-	7.63±0.03	7.56-7.6	7.63±0.02	7.56-7.66
III. $PM_{2.5}$ and meteorological parameters						
$PM_{2.5}$ (μg m^{-3})	34±37	0.2−107	104±60	80−272	114±44	74−192
RH (%)	21±7.3	6.1−67	41±17	15−72	56±14	22−72
T (^OC)	0.4±3.0	-5.9−9.0	1.4±2.8	-3.7−8.9	0.9±2.6	-1.7−8.2
Visibility (km)	40±14	8.3−50	7.1±2.4	4.1−19	2.9±0.8	1.9−5.0

Table S3. Detection of sulfate formation in the reaction cell

Experimental run	SO_2 (350 ppm)	NO_2 (350 ppm)	Water	3 wt % NH_3	Integrated sulfate desorption peak area (x 10^6 cps)
1 (3)	In N_2	In N_2	√	x	6.8±2.6
2 (3)	In N_2	In N_2	x	√	11.0 ±4.3
3 (1)	In air	In air	√	x	6.5
4 (1)	In air	In air	x	√	10.0

The symbols "√" and "x" indicate whether a water or NH_3 solution was used and not used in the exposure, respectively. The number in parenthesis on the right column denotes the number of repeating experiments.

Table S4. Detection of particle growth and sulfate formation in the reaction chamber

Experimental run	SO_2 (250 ppb)	NO_2 (250 ppb)	NH_3 (1 ppm)	Water vapor (70% RH)	Sulfate formation (m/z=96)	Particle growth
1	√	x	x	√	No	No
2	√	x	√	√	No	No
3	√	√	√	√	Yes	Yes
4	√	√	x	√	No	No
5	√	√	√	x	No	No

The symbols "√" and "x" indicate whether a species is included or excluded in the exposure, respectively.

Table S5. Uptake coefficient (γ) of SO_2 on aerosols during Beijing 2015

	Average $[SO_4^{2-}]$ ($\mu g\ m^{-3}$)	RH (%)	N ($x10^4$) (cm^{-3})	Average D_p (nm)	S ($\times10^{-5}$) ($cm^2\ cm^{-3}$)	$[SO_2(g)]$ (ppb)	$d[SO_4^{2-}]$ ($\mu g\ m^{-3}$)	dt (hr)	γ ± 1σ
Clean	4	21	7.5	75.0	1.3	16.3	3.0	7.2	$(1.6\pm0.7)\times10^{-5}$
Transition	14	41	9.0	114.2	3.7	24.2	12.7	6.0	$(2.1\pm1.6)\times10^{-5}$
Polluted	26	56	8.1	116.2	3.4	16.2	14.7	7.0	$(4.5\pm1.1)\times10^{-5}$

Table S6. Uptake coefficient (γ) of SO_2 on oxalic acid particles in the reaction chamber

RH (%)	D_o (nm)	D_p/D_o	N (cm^{-3})	S ($\times10^{-5}$) ($cm^2\ cm^{-3}$)	$[SO_2(g)]$ (ppb)	dt (min)	γ ± 1σ
30	45	1.06	1.0×10^3	1.3	250	60	$(6.7\pm9.1)\times10^{-6}$
65	45	1.5	1.0×10^3	4.0	250	60	$(8.3\pm5.7)\times10^{-5}$
70	45	2.31	1.0×10^3	3.4	250	60	$(3.9\pm1.2)\times10^{-4}$